Volume 22, No 2 | International Journal of Radiation Research, April 2024

Spectral CT based radiomics for predicting brain metastases in patients with lung cancer

S. Cao* and Z. Shu

Department of Radiology, Shanghai Traditional Chinese Medicine-Integrated Hospital, Shanghai 200082, China

► ***Original article***

Corresponding author:
Shengnan Cao, M.M.,
E-mail:
cao906436987@163.com

Received: June 2023
Final revised: June 2023
Accepted: July 2023

Int. J. Radiat. Res., April 2024; 22(2): 347-353

DOI: 10.61186/ijrr.22.2.347

Keywords: *Prediction model, spectral CT, radiomics, lung cancer, brain metastasis.*

ABSTRACT

Background: The goal of this study was to create a prediction model for brain metastasis (BrMs) in patients with lung cancer using unenhanced spectral computed tomography (CT) and radiomics. ***Materials and Methods:*** This study comprised 162 patients with lung cancer who underwent spectral CT from 2019–2021. Patients were split into training and test sets and into BrMs and BrMs-free groups. Spectral and radiomics parameters were obtained from the spectral CT images before pathological confirmation. Prediction models in the training and test sets were created using logistic regression. The receiver operating characteristic curve was used to evaluate each quantitative parameter for predicting BrMs. The diagnostic effectiveness of several parameters was analyzed and compared using the area under the curve (AUC) calculation. The final model was obtained using the Delong test. ***Results:*** There were statistically significant differences in the iodine concentrations and the slope of the energy spectrum attenuation curve of the two groups <(p0.05). The AUC of the combined radiomics model was greater than that of the 70 keV and 120 keV sequence models. The joint parameters of radiomics and spectral CT constructed an integrated model. In the training set, test set, and overall set, the AUCs of the integrated model were 0.875, 0.879, and 0.724, respectively. In the training and overall sets, the prediction performance of the integrated model outperformed the spectral and radiomics models (p<0.05). ***Conclusions:*** This integrated model may predict the BrMs in lung cancer patients.

INTRODUCTION

One of the most aggressive cancers, lung cancer, affects people all over the world [1]. According to estimates, it will continue to be the top cause of cancer death in 2020, accounting for 11.4% of the 19.3 million new cancer cases [2]. Brain metastases (BrMs) in lung cancer patients are common, particularly those with non-small cell lung cancer (NSCLC), nearly 50% of cases had BrMs [3]. BrMs are linked to marked morbidity and high mortality [4-5]. It is worth mentioning that according to previous studies, early local therapies or therapies combined with systemic treatment may offer better intracranial progression-free survival [3]. However, the methods for predicting the occurrence of BrMs are rarely reported and not always accurate.

Spectral computed tomography (CT) can obtain information from a virtual plain scan image, material separation image, single energy spectrum image, effective atomic number image, and energy spectrum curve. Spectral CT has a lot of applications in lung cancer. Using energy spectrum data, benign and cancerous lung lesions can be identified, mediastinal lymph node metastasis can be detected before surgery, lung cancer can be classified and staged, the epidermal growth factor receptor (EGFR) status of NSCLC can be anticipated, and lung cancer angiogenesis and prognosis can be assessed [6-10]. It also helps to determine whether pure ground-glass nodules are invasive [11].

Radiomics was first proposed by Dutch researchers Lambin *et al.* [12]. Radiomics refers to a high throughput extraction of many features from images, resulting in diagnosis, prognosis, and prediction models. Radiomics can be applied in various biomedical fields. It is widely used in oncology, especially in advanced cancer, having the potential for individualized tumor treatment [13]. According to a study, for patients with locally advanced non-small cell lung cancer (LA-NSCLC) who had undergone curative surgery, the integrated nomogram may be the best tool for predicting BrMs-free survival when paired with the clinical and CT radiomics features [14]. However, studies on spectral CT image-based lung cancer radiomics are rare.

In this study, the authors attempt to create and evaluate a prediction model by combining pre-treatment spectral CT radiomics features of primary lung cancer with quantitative parameters of energy spectrum. This model may provide a new method for the early detection of BrMs in lung cancer patients.

[DOI: 10.61186/ijrr.22.2.347]

MATERIALS AND METHODS

Patient population

The study received an exemption from ethical review by the Institutional Review Board of Shanghai Traditional Chinese Medicine-Integrated Hospital, as this was a retrospective study. The principles of the Helsinki Declaration are adhered to in this research. We evaluated 162 lung cancer cases diagnosed pathologically at our facility between January 2019 and April 2021. Lung cancer (pathological results were obtained by operation or puncture) and having had spectral CT scanning before treatment were the inclusion criteria. Following were the exclusion criteria: nodules with a diameter less than 5 mm (N = 16); poor spectral image quality or image data error, which could not satisfy further analysis (N = 15); absence of follow-up data (N = 49). A 4:1 ratio was used to randomly split these included lung cancer patients into training and test sets.

Follow-up status

BrMs, the primary measurement outcome of this research, were defined as the time interval between the dates of spectral CT scanning (before pathological diagnosis) and the BrMs, or the last date patients were known to be BrMs-free. The follow-up period came to an end in June 2021. Patients were followed up every 3 to 6 months, or following the medical advice. The occurrence of BrMs was mainly determined by craniocerebral CT or magnetic resonance imaging (MRI) scanning (including ours and another institution). The patient's medical records provided the information above and the baseline clinical data. Part of the information was obtained by telephone follow-up.

Technical specifications for acquiring spectral CT images

The gemstone spectral CT (General Electric Company, Revolution 256CT, USA) was used to scan the chest. The patients were asked to perform routine respiratory training in the supine posture before the scan. The upper boundary of the scanning range was thyroid cartilage, and the lower boundary was the costophrenic angle. The mediastinal window images were transmitted to the GE Advantage Workstation 4.7(GE Healthcare, USA). Image analysis was done with the built-in gemstone spectral imaging (GSI) viewer software package. The following were the dual-energy CT scanning parameters: “A” tube voltage is 70 kVp, “B” tube voltage is 120 kVp, the tube current is 365 mA, the automatic milliampere technology switches instantaneously to 0.5 ms, the layer thickness and spacing are both set to 5 mm, the pitch is 0.984, and the collimator is set to 64*0.625. The gemstone spectral CT scanning utilizes the characteristics of different substances with varying attenuation coefficients under different ray energies for imaging. Usually, substances with different levels of attenuation are chosen to form a base material pair. Water and iodine are commonly used combinations because they encompass a range of common substances in human medicine.

Acquisition of image quantitative parameters

Without knowing the pathology, two radiologists collected the quantitative parameters independently at the General Electric Company Advantage Workstation 4.7 (GE Healthcare, USA). These radiologists had more than 10 years of experience. When there were differences among the results, a consensus was reached through negotiation. The GSI viewer software can automatically generate the iodine and water-based substance separation images. By outlining the region of interest (ROI), this software can automatically calculate its water concentration (WC) and iodine concentration (IC). GSI viewer software can also automatically calculate CT values of all single energy images and form an energy spectrum attenuation curve for each ROI. The Greek alphabet letter λ represented the slope of the energy spectrum attenuation curve. The λ of the target lesion was calculated using the equation (λHU): $\lambda HU=(CT_{40keV}-CT_{90keV})/50$. The ROI setting area was 30 $mm^{2,}$ and the propagation was set to all volumes to ensure consistency. The ROI was placed in the largest slice of the target lesion and in the uniform tissue composition. All ROI were measured thrice, and the average value was taken (figure 1).

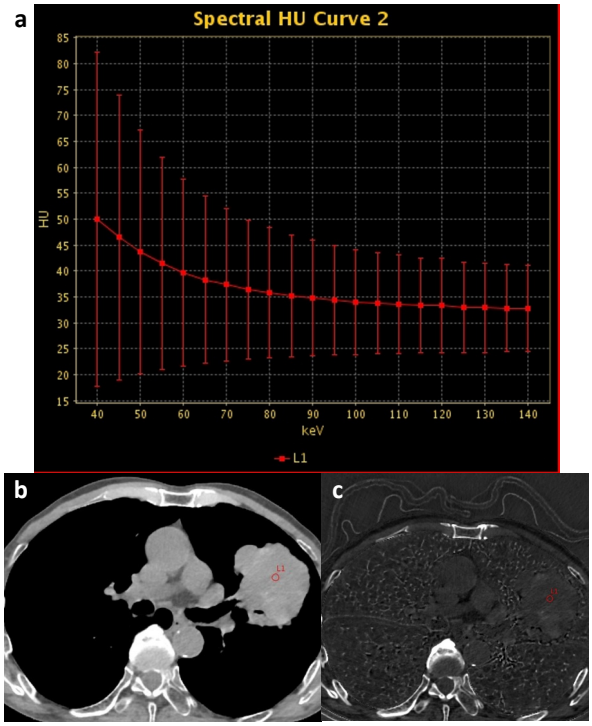

Figure 1. In the post-processing, radiologist drew the ROI in the iodine and water-based substance separation image and obtained the spectral curve, WC, and, IC. **a:** Spectral Curve; **b:** Water (Iodine) image; **c:** Iodine (Water) image.

[DOI: 10.61186/ijrr.22.2.347]

Radiomics feature extraction and analysis

The ROI was randomly drawn by two experienced radiologists on the largest lesion level in two dimensions. Subsequently, radiomics features were extracted using radiomics software (Beijing Yizhun AI Technology Company, CHN). One imaging technologist with more than 3-year working experience reconstructed 70 keV and 120 keV sequences through standardized post-processing software. The reconstructed layer thickness and layer spacing were 0.625 mm, and the DICOM data were imported into the scientific research platform. Before delineating the ROI, we set a unified standard. The ROI must be delineated along the tumor's margin while avoiding large blood vessels, bronchi, and calcification as much as possible (figure 2). Based on each patient's unenhanced spectral CT images, 1878 features were recovered, comprising 939 features of the 70 keV and 120 keV sequences, respectively. The main categories of feature were: first order statistics; shape based; gray level cooccurrence matrix; gray level run length matrix; gray level size zone matrix; neighboring gray tone difference matrix of original, and wavelet-based features. Three models were constructed, including 70 keV sequence, 120 keV sequence, and combined sequence. The first-dimension reduction of each model was performed by a statistical method, and then the second-dimension reduction was carried out using the logistic regression method.

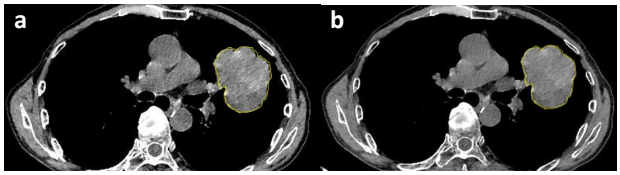

Figure 2. Radiologists drew the ROI on the largest lesion level in two dimensions in 70 keV and 120 keV sequences. ROI was outlined along the edge of the tumor. **a:** 70 keV sequences; **b:** 120 keV sequences.

Statistical validation

All quantitative data were analyzed by the SPSS 22.0 software package (IBMCorp., Armonk, N.Y., USA)) and the MedCalc Statistical Software version 19.3.1 (MedCalc Software Ltd, Ostend, Belgium). The measurement data were all mean ± Standard deviation representation. A chi-square test was used to compare the count data between the training and test sets. The independent two-sample T-test was used to examine the quantitative parameters, including age, IC, WC, and λHU. The difference was statistically significant ($P<0.05$). The most valuable features from the quantitative spectral parameters and radiomics features in the training set were selected using the logistic regression model. These parameters were used to construct the models, including the spectral, radiomics, and integrated model. From the 70 keV and 120 keV sequences, the radiomics model was chosen. Each patient's rad-score was calculated using a linear combination of selected features. Furthermore, these selected features were weighted by their respective coefficients. The effectiveness of the rad-score for predicting BrMs for the training set, test set, and overall set was assessed using ROC. The AUC was calculated to analyze and compare the effectiveness of various parameters as diagnostic indicators. The final model was obtained using the Delong test, and the best model was verified in 5-fold cross-certification.

RESULTS

The flowchart of the study is presented in figure 3.

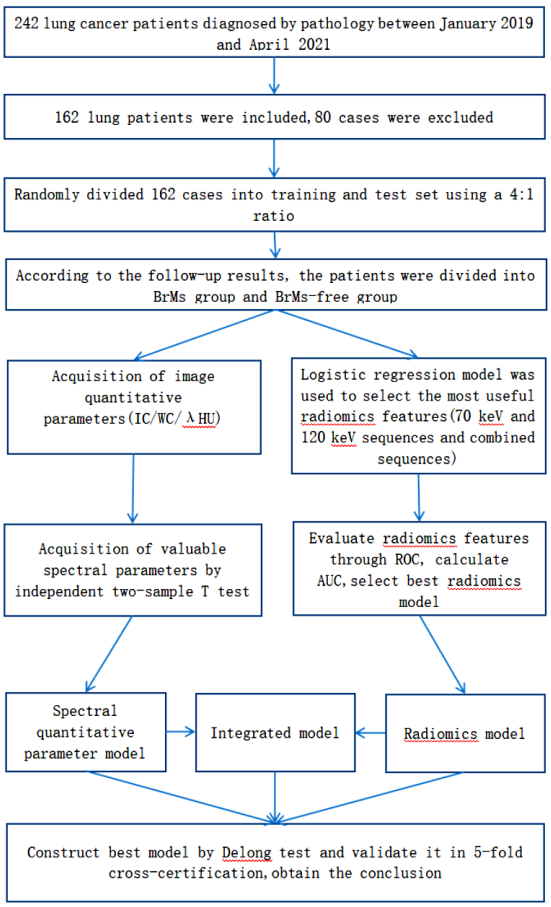

Figure 3. Flowchart of this study. The inclusion criteria: 1. Lung cancer (pathological results were obtained by operation or puncture); 2. Underwent spectral CT scanning before treatment. The exclusion criteria: 1. Ground-glass nodules with a small volume (N = 16); 2. Poor spectral image quality or image data error that could not satisfy further analysis (N = 15); 3. Lack of follow-up information (N = 49).

Patients and follow-up

Table 1 displays the characteristics of the studied groups. Among the lung cancer patients, the median age was 65.1 years. Approximately 65.4% were male, and the BrMs group had a greater percentage of both males and older age than the BrMs-free group did ($p<0.05$). Table 2 summarizes the clinical

[DOI: 10.61186/ijrr.22.2.347]

characteristics and spectral parameters in the training and test sets. Age, sex, IC, WC, and HU did not differ significantly (p>0.05). In the overall cohorts, the follow-up duration was 12.62±9.21 months. Among these patients, BrMs occurred in 25 patients (15.4%), with the median BrMs duration 2.92±4.64 months. Approximately 76% of BrMs occurred in 1 month, 80% occurred in 3 months, and 88% occurred in 6 months.

Table 1. General information.

		group		T/X^2 VALUE	P VALUE
		BrMs group (25)	BrMs-(free137)		
Sex	male	11	95	6.003	0.014
	female	14	42		
Age		60.96±9.17	65.85±8.81	-2.538	0.012

Table 2. Spectral characteristics of patients of lung cancer in the training set and test set.

	TRAINING SET (N=129)	TEST SET (N=33)	T/X^2 VALUE	P VALUE
AGE	64.67±9.12	66.79±8.52	-1.208	0.229
SEX (MALE/ FEMALE)	89/40	23/10	0.006	0.938
IC	5.46±3.06	5.30±3.04	0.259	0.796
WC	1018.92±80.46	1026.02±9.40	-0.504	0.615
L VALUE	0.74±0.42	0.72±0.41	0.248	0.804

Spectral parameters selection

According to the follow-up results, 162 patients were separated into BrMs and BrMs-free groups. Statistics showed a significant difference in the values of λHU and IC between the two groups (p<0.05). Lung cancer patients in the BrMs group had higher HU and IC values than in the BrMs-free group. Nevertheless, between the two groups, there was no significant difference in the value of WC (table 3). The WC value had no distinguishing value for these two groups.

Table 3. Spectral parameters in the BrMs group and BrMs-free group.

	BRMS GROUP	BRMS-FREE GROUP	T VALUE	P VALUE
WC	1027.95±10.31	1018.98±78.05	0.572	0.568
IC	6.79±2.81	5.18±3.04	2.475	0.014
L VALUE	0.92±0.39	0.70±0.41	2.490	0.014

Construction and evaluation of radiomics models based on spectral CT images

By dimensionality reduction, these three models (70 keV, 120 keV, and the combined sequence model) obtained 20, 19, and 21 features respectively. After calculating each rad-score, the AUC of 70 keV sequence model were 0.637 for the training set and 0.621 for the test set, the AUC of 120 keV sequence model were 0.766 and 0.764, while the AUC of combined sequence model were 0.793 and 0.771. Other indexes, including precision, sensitivity, and specificity are listed in table 4. The AUC and precision of combined sequence model were similar with 70 keV sequence model but slightly higher than 120 keV sequence model in the training set. As we expected, in the test set, the AUC of combined sequence model were similar with 70 keV sequence model but slightly higher than 120 keV sequence model. Meanwhile, the precision of combined sequence model was higher than 70 keV and 120 keV sequence models in the test set. These results indicated the trend that the prediction efficiency of combined model was more effective than that of 70 keV and 120 keV sequence models (figure 4). In addition, in the test set, 120 keV sequence model had high sensitivity but poor specificity, while the sensitivity and specificity of combined model performed well. Therefore, combined model was considered the best radiomics model. After dimensional reduction by logistic regression analysis, twenty potential predictors were left (figure 5).

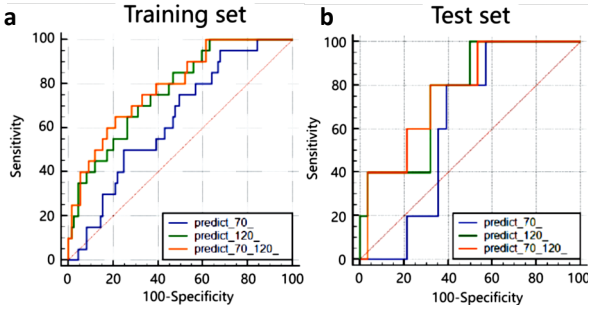

Figure 4. a: ROC of 70 keV sequence model, 120 keV sequence model, combined model (70 keV sequence + 120 keV sequence) in training set; **b:** ROC of 70 keV sequence model, 120 keV sequence model, combined model in test set.

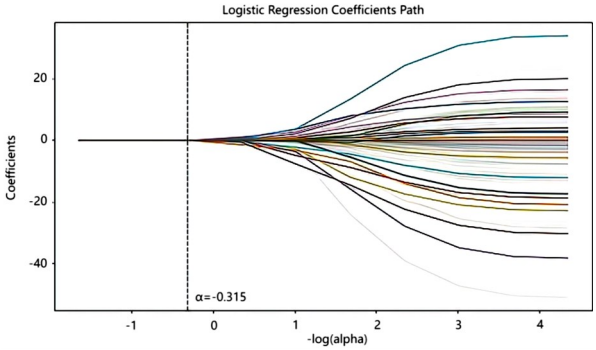

Figure 5. The After dimensional reduction by logistic regression analysis, twenty potential predictors were left. The value of log (alpha) while choosing the ideal number of features is shown by the dashed line. α=-0.315.

Table 4. Prediction performance of 70 keV sequence, 120 keV sequence and combined models in training set and test set.

	AUC(P value, 95% CI)	Precision	Sensitivity	Specificity
Training set				
70 keV sequence	0.637(0.0248, 0.547–0.720)	0.54	95.0	32.0
120 keV sequence	0.766(<0.0001, 0.683–0.836)	0.65	70.0	68.8
70+120 keV sequence	0.793(<0.0001, 0.706–0.854)	0.67	65.0	78.9
Test set				
70 keV Sequence	0.621(0.2189, 0.436–0.784)	0.55	100.0	42.9
120 keV sequence	0.764(0.0153, 0.585–0.894)	0.61	100.0	50.0
70+120 keV sequence	0.771(0.0117, 0.593–0.899)	0.70	80.0	67.9

[DOI: 10.61186/ijrr.22.2.347]

Performance evaluation and validation of S, R, and S+R models

The S, R, and S+R represent the radiomics model, spectral model and integrated model, respectively. In the training and test sets, the AUC of the S model were 0.708 (p=0.0003, 0.621–0.785, 95% CI) and 0.793 (p=0.0002, 0.617–0.914, 95% CI), respectively. The AUC of the R model were 0.787 (p<0.0001, 0.706 –0.854, 95% CI) and 0.771 (p=0.0117, 0.593–0.899, 95% CI), respectively. The AUC of the S + R model were 0.875 (p<0.0001, 0.806–0.927, 95% CI) and 0.879 (p<0.0001, 0.718–0.966, 95% CI), respectively (figure 6).

The prediction performances of S and R models were similar, and no statistically significant difference could be found between the two (training set p=0.3155, test set p=0.8815, overall set p=0.4001). In the training set, compared to the S and the R model, the prediction performance of S+R model is significantly better (p=0.0051 for the S and S+R model, p =0.0129 for the R and S+R model). However, the test set showed no statistically significant differences (p=0.0770 for the S and S+R model, p=0.3964 for the R and the S+R model). Nevertheless, the AUC of S+R model was higher than S and R model. This still indicated a trend that the S+R model was slightly better than S and R models. Moreover, in the overall set, compared to the S model and the R model, the prediction performance of S+R model was better (p=0.0012 for the S and S+R model, p =0.0093 for the R and S+R model) (table 5). The S+R model underwent a 5-fold cross-certification, and the AUC value of mean ROC was 0.74 (figure 6).

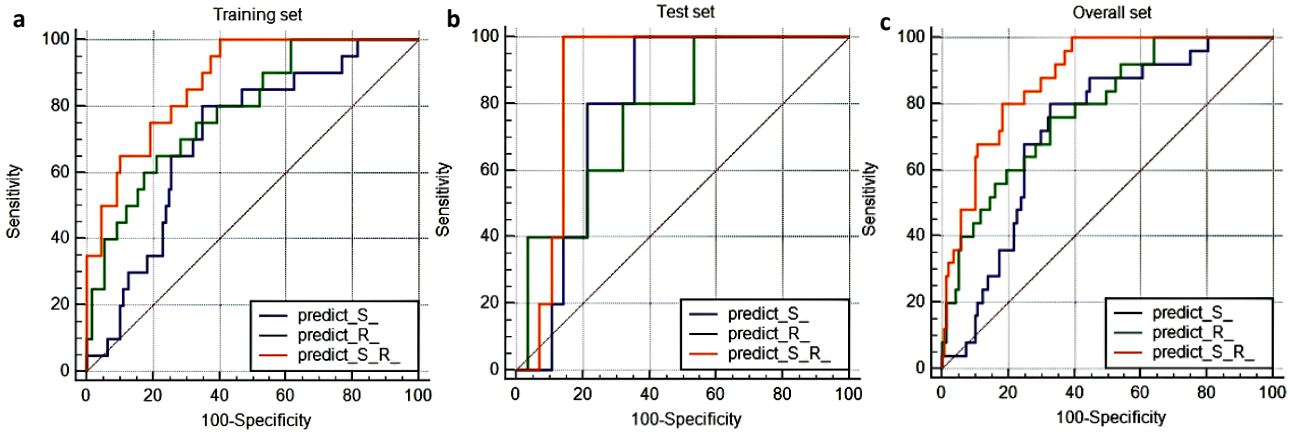

Figure 6. Spectral model, R: radiomics model, S + R: integrated model; **(a):** ROC of S model, R model, S + R model in training set; **(b):** ROC of S model, R model, S + R model in test set; **(c):** ROC of S model, R model, S + R model in overall set.

Table 5. Prediction performance of S,R and S+R models in training, test and overall sets.

	Training set				Test set				Overall set			
	AUC P value 95% CI	P			AUC P value 95% CI	P			AUC P value 95% CI	P		
		S	R	S+R		S	R	S+R		S	R	S+R
S	0.708 0.0003, 0.621-0.785	-	0.3155	0.0051	0.793 0.0002, 0.617-0.914	-	0.8815	0.0770	0.724 <0.0001, 0.649-0.792		0.4001	0.0012
R	0.787 <0.0001, 0.706-0.854	-	-	0.0129	0.771 0.0117, 0.593-0.899	-	-	0.3964	0.782 <0.0001, 0.710-0.843			0.0093
S+R	0.875 <0.0001, 0.806-0.927	-	-	-	0.879 <0.0001, 0.718-0.966	-	-	-	0.879 <0.0001, 0.819-0.925			

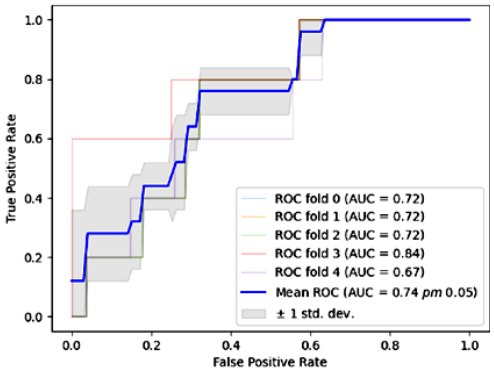

Figure 7. Model validation (5-fold cross-certification).

[DOI: 10.61186/ijrr.22.2.347]

DISCUSSION

The value of spectral CT in lung cancer is reflected in the qualitative, classification, staging, and prognosis evaluation. The research on the prognostic utility of spectral CT has mainly focused at lymph node metastasis and bone metastasis for lung cancer [16-17]. The detection of BrMs of lung cancer usually depends on the clinical manifestations combined with MRI or CT examination. Studies on the risk factors of BrMs always focus on clinical features. Epidermal growth factor receptor, anaplastic lymphoma kinase, or rearranged during transfection gene status are also considered as high risk factors for predicting BrMs in lung cancer [18-19]. One investigation has confirmed that BrMs in stage IA peripheral small cell lung cancer (SCLC) patients can be predicted by the thickness of the bronchovascular bundle on CT [20]. The necrosis rate of lesions pheralis that lead to lung cancer brain and bone metastasis [21].

The findings of this study demonstrated the existence of significant differences in λHU and IC, but not in WC between BrMs and BrMs-free groups. The author believes that IC and λ are potential predictors of BrMs risk in lung cancer. In different research directions, λHU, IC, and WC have different values when evaluating spectral CT in lung cancer. Energy spectrum parameters based on enhanced scanning might provide more valuable parameters. Only unenhanced images were selected in this study because they were easy to obtain, and could accommodate patients with allergies or intolerance contrast media.

Identifying tumor metastasis is one of the most significant tasks of tumor molecular imaging. For example, intracranial tumorigenicity of lung tumor cells is increased by the phenotypic plasticity of the BrMs microenvironment [22]. The circadian rhythm regulator hepatic leukemia factor is downregulated, which encourages the multiple organ distant metastasis of NSCLC [23]. Although the molecular imaging of metastasis has made substantial progress as a field of clinical research, its accuracy needs to be verified. CT, Positron Emission Tomography-CT, MRI and other imaging methods are more difficult to predict the potential of BrMs; thus, and radiomics has become a prominent topic in recent years. The predictive significance of CT and MRI imaging features on the survival rate of BrMs of NSCLC has been supported by some studies [24-25]. However, these studies were based on the specific BrMs that have been found, and the research subjects were metastatic tumors, not lung cancer lesions themselves. However, the survival rates of patients with early NSCLC are highly correlated with radiomics, according to a few research [26].

Based on the features, CT imaging can potentially predict BrMs of lung cancer [27]. This findings of this study showed that unenhanced spectral CT (70 keV and 120 keV sequence models) could also predict the likelihood of BrMs, and the combined model was slightly better.

Although radiomics has many advantages, it does not need more examination time or costs. It is a more accurate diagnosis without increasing pain in patients. However, it has some shortcomings for a long time, such as the incomprehensible and unreadable features and the poor consistency and repeatability in various studies. In this study, we tried to combine radiomics features with quantitative parameters of spectral CT to establish an integrated model to increase the readability. The results in the training set showed that the combined S+R model is better than S and R model in predicting BrMs. Although this trend is only indicated in the test set, the prediction performance is still good in the overall set. Therefore, we believe the S + R model may be a new prediction model for lung cancer patients.

This study has a few drawbacks. First, since this was a retrospective study with participants only from our institution, selection bias might be present. Second, among 162 patients, only 25 had BrMs; thus, the sample size was limited. Third, the follow-up time was short, and the clinical parameters including smoking index, TNM stage, pathological grade, and treatment plan were not included in the study due to incomplete data. Other related genes, such as EGFR and ALK, were not included in the study. Further research and verification are needed in the future.

In conclusion, patients with BrMs frequently have elevated IC and λHU. The spectral CT-based radiomics model performed well in predicting BrMs. Furthermore, the integrated model incorporating radiomics features and spectral CT parameters appears to be more favorable for predicting BrMs. In the future, we may develop a more advanced model to categorize lung cancer patients' risk, and treat the high-risk population earlier to raise patient survival rates.

ACKNOWLEDGMENTS

The authors thank the reviewers for their critical feedback and helpful comments.

***Funding*:** The authors got financial support from "Youth Talent Training Plan" of Shanghai Traditional Chinese Medicine-Integrated Hospital Affiliated to Shanghai University of Traditional Chinese Medicine. (Project No: RCPY0061A)

***Conflicts of interest statement*:** The authors had no conflicts of interest to declare

***Author contribution*:** All authors read and approved the final manuscript. Shengnan Cao and Zheng Shu conceived and designed this study. Shengnan Cao collected important background data and drafted the manuscript.

***Funding*:** No funding has been received for this study.

[DOI: 10.61186/ijrr.22.2.347]

REFERENCES

1. McGuire S (2015) World Cancer Report 2014. Geneva, Switzerland: World Health Organization, International Agency for Research on Cancer, WHO Press. *Adv Nutr, **7**: 418-9.*
2. Sung H, Ferlay J, Siegel RL, *et al.* (2021) Global Cancer Statistics 2020: GLOBOCAN Estimates of Incidence and Mortality Worldwide for 36 Cancers in 185 Countries. *CA Cancer J Clin, **71**:209-249.*
3. Page S, Milner-Watts C, Perna M, *et al.* (2020) Systemic treatment of brain metastases in non-small cell lung cancer. *Eur J Cancer, **132**:187-198.*
4. Sperduto PW, Kased N, Roberge D, *et al.* (2012) Summary report on the graded prognostic assessment: an accurate and facile diagnosis -specific tool to estimate survival for patients with brain metastases. *J Clin Oncol, **30**:419e25.*
5. Sacks P and Rahman M (2020) Epidemiology of brain metastases. *Neurosurg Clin N A, **31**:481-488.*
6. Wen Q, Yue Y, Shang J, *et al.* (2021) The application of dual-layer spectral detector computed tomography in solitary pulmonary nodule identification. *Quant Imaging Med Surg, **11**:521-532.*
7. Fehrenbach U, Kahn J, Böning G, *et al.* (2019) Spectral CT and its specific values in the staging of patients with non-small cell lung cancer: technical possibilities and clinical impact. *Clin Radiol, **74**456-466.*
8. Zhu Q, Ren C, Zhang Y, *et al.* (2020) Comparative imaging study of mediastinal lymph node from pre-surgery dual energy CT versus post-surgeron verifications in non-small cell lung cancer patients. *J Peking Univ Health Sci, **52**: 730-737.*
9. Zhang G, Cao Y, Zhang J, *et al.* (2021) Epidermal growth factor receptor mutations in lung adenocarcinoma: associations between dual-energy spectral CT measurements and histologic results. *J Cancer Res Clin Oncol, **147**:1169-1178.*
10. Li Q, Li X, Li XY, *et al.* (2020) Spectral CT in Lung Cancer: Usefulness of Iodine Concentration for Evaluation of Tumor Angiogenesis and Prognosis. *AJR Am J Roentgenol, **215**:595-602.*
11. Yu Y, Cheng JJ, Li JY, *et al.* (2020) Determining the invasiveness of pure ground-glass nodules using dual-energy spectral computed tomography. *Transl Lung Cancer Res, **9**: 484-495.*
12. Lambin P, Rios-Velazquez E, Leijenaar R, *et al.* (2012) Radiomics: extracting more information from medical images using advanced feature analysis [J]. *Eur J Cancer, **48**:441-446.*
13. Song J, Yin Y, Wang H, *et al.* (2020) A review of original articles published in the emerging field of radiomics[J]. *Eur J Radiol, **127**: 108991.*
14. Sun F, Chen Y, Chen X, *et al.* (2021) CT-based radiomics for predicting brain metastases as the first failure in patients with curatively resected locally advanced non-small cell lung cancer. *Eur J Radiol, **134**:109411.*
15. Lennartz S, Mager A, Große Hokamp N, *et al.* (2021) Texture analysis of iodine maps and conventional images for k-nearest neighbor classification of benign and metastatic lung nodules. *Cancer Imaging, **21**:17.*
16. Yang F, Dong J, Wang X, *et al.* (2017) Non-small cell lung cancer: Spectral computed tomography quantitative parameters for preoperative diagnosis of metastatic lymph nodes. *Eur J Radiol, **89**:129-135.*
17. Yue D, Ru Xin W, Jing C, *et al.* (2017) Virtual monochromatic spectral imaging for the evaluation of vertebral inconspicuous osteoblastic metastases from lung. *Acta Radiol, **58**:1485-1492.*
18. Won YW, Joo J, Yun T, *et al.* (2015) A nomogram to predict brain metastasis as the first relapse in curatively resected non-small cell lung cancer patients. *Lung Cancer, **88**: 201-7.*
19. Wang H, Wang Z, Zhang G, *et al.* (2020) Driver genes as predictive indicators of brain metastasis in patients with advanced NSCLC: EGFR, ALK, and RET gene mutations. *Cancer Med, **9**:487-495.*
20. Sung P, Yoon SH, Kim J, *et al.* (2021) Bronchovascular bundle thickening on CT as a predictor of survival and brain metastasis in patients with stage IA peripheral small cell lung cancer. *Clin Radiol, **76**:76.e37-76.e46.*
21. Hwang KE, Oh SJ, Park C, *et al.* (2018) Computed tomography morphologic features of pulmonary adenocarcinoma with brain/bone metastasis. *Korean J Intern Med, **33**:340-346.*
22. Wei XG, Bi KW, Li B (2021) Phenotypic Plasticity Conferred by the Metastatic Microenvironment of the Brain Strengthens the Intracranial Tumorigenicity of Lung Tumor Cells. *Front Oncol, **11**: 637911.*
23. Chen J, Liu A, Lin Z, *et al.* (2020) Downregulation of the circadian rhythm regulator HLF promotes multiple-organ distant metastases in non-small cell lung cancer through PPAR/NF-κb signaling. *Cancer Lett, **482**: 56-71.*
24. Zhang J, Jin J, Ai Y, Zhu K, Xiao C, Xie C, Jin X. (2021) Computer Tomography Radiomics-Based Nomogram in the Survival Prediction for Brain Metastases From Non-Small Cell Lung Cancer Underwent Whole Brain Radiotherapy. *Front Oncol, **10**:610691.*
25. Zhao S, Hou D, Zheng X, *et al.* (2021) MRI radiomic signature predicts intracranial progression-free survival in patients with brain metastases of ALK-positive non-small cell lung cancer. *Transl Lung Cancer Res, **10**: 368-380.*
26. Huang Y, Liu Z, He L, *et al.* (2016) Radiomics Signature: A Potential Biomarker for the Prediction of Disease-Free Survival in Early-Stage (I or II) Non-Small Cell Lung Cancer. *Radiology, **281**:947-957*
27. Chen A, Lu L, Pu X, *et al.* (2019) CT-Based Radiomics Model for Predicting Brain Metastasis in Category T1 Lung Adenocarcinoma. *AJR Am J Roentgenol, **213**:134-139*.

[DOI: 10.61186/ijrr.22.2.347]